Scaling resistance by fluoro-treatments: The importance of wetting states

Li Liu[1,2,3], Laura Charlton[4], Yanqing Song[4], Tao Li[2], Xuemei Li[1], Huabing Yin[4]*, Tao He[1]*

[1]Shanghai Advanced Research Institute, Chinese Academy of Sciences, Shanghai 201210, China

[2]School of Physical Science and Technology, ShanghaiTech University, Shanghai 201210, China

[3]University of Chinese Academy of Sciences, Beijing 100049, China

[4] James Watt School of Engineering, University of Glasgow, Glasgow G12 8LT, UK

*Corresponding authors: het@sari.ac.cn, huabing.yin@glasgow.ac.uk

Abstract

Membrane distillation is a thermally driven separation process using hydrophobic, porous membranes. Among various problems faced by membrane distillation, scaling remains an unresolved challenge in treating streams of high salinity. Development of superhydrophobic membranes has been a central approach to address this, with CF4 plasma treatment or fluorochemical modification commonly used. However, contradictory observations often occur where some membranes are scaling resistant, but others are not. For the first time, we examine this issue by systematic comparison of the impacts of commonly used fluoro-treatments on scaling resistance. A state-of-the-art surface patterned micro-pillared poly (vinylidene fluoride) membrane (MP-PVDF) was used and both CF4 plasma and fluorosilane reagents were utilized to enhance membrane hydrophobicity. The resulted membranes CF4-MP-PVDF (by CF4 plasma) and FAS-MP-PVDF (via fluorosilane) were systematically characterized and their anti-scaling performance was evaluated using a supersaturated $CaSO_4$ solution. Although both modified membranes showed increased water contact angle, reduced sliding angle and surface energy, CF4-MP-PVDF demonstrated better scaling resistance than FAS-MP-PVDF. Conventional thermodynamic nucleation models dictate similar nucleation energy barriers for both, in discrepancy to experimental observations. Instead, the wetting states and hydraulic surface slippage were identified as the determinant factors. The CF4-MP-PVDF in a suspended-wetting state with slippage resisted scaling robustly, while FAS-MP-PVDF in an unstable transition state and pristine MP-PVDF in a pinned state were suspectable to scaling. These results unravel, for the first time, the fundamental mechanism behind the differences in scaling resistance by CF4 plasma treatment and fluorosilane surface modification.

Keywords: Membrane distillation, Wetting state, Slip length, Scaling resistance, Nucleation

1. Introduction

Membrane distillation (MD) is a thermal separation process based on hydrophobic porous membranes and driven by a vapor pressure gradient [1, 2]. MD is not sensitive to salt concentrations, thus it is capable of treating liquids of high salinity. For industries where low-grade thermal energy is largely available, MD processes are promising for concentrating hypersaline fluids before final spray drying of the salt products as well as for achieving near-Zero Liquid Discharge (nZLD) in wastewater management [3-5]. However, the scaling caused by inorganic matter and consequent wetting and deteriorated performance limit the large-scale application of MD in real-world settings.

Sparsely soluble salts in hypersaline water often precipitate out during concentration processes, leading to ubiquitous scaling problems [3, 6]. In a membrane-based desalination process, nuclei and crystals formed in bulk feed solution (called homogeneous nucleation) or grown on membrane surfaces (called heterogeneous nucleation) lead to extra mass transfer resistance, resulting in declined flux [7, 8]. Some strategies such as the addition of antiscalants [9-11] or upstream coagulation and softening [12] can delay the occurrence of scaling, but frequently induce secondary contamination or cause difficulty in the post-treatment of concentrate solutions [13-15]. Nanofiltration (NF) has demonstrated effective mitigation of scaling by removing multivalent ions [13, 16], but this mainly relocates the scalants to the NF membranes. Furthermore, the additional nanofiltration system increases the cost of the whole treatment process. Recent use of process adjustment, such as feed pulse flow [17, 18], nanobubbles [19, 20] or gas purging [21] have also demonstrated promise in scaling control. These process optimizations obey the fact that scaling occurs at the membrane-liquid interface, thus it is fundamentally an interfacial

issue closely related to the physiochemical characteristics of the membrane materials and the interplay between the liquid and membrane surface [3].

Inspired by the self-cleaning property of lotus leaves [22], many researchers have explored the design of biomimetic surfaces and wetting behavior models to create superhydrophobic membranes to achieve desirable scaling resistance [23-31]. A superhydrophobic membrane often possess lower surface energy, which can be achieved via chemical fluorination modification [32, 33], or CF4 physical treatment [34-36]. Minimizing the liquid solid contact area is also important, which can be achieved by introducing hierarchical structure [31, 37-39] or increasing surface porosity [40, 41]. Although most current superhydrophobic membranes show good anti-scaling properties, there are some contradictory results, where some membranes are scaling resistant, but others not [21, 26, 42].

Current understanding of MD scaling is mainly built on the interpretation of thermodynamics. Classical nucleation and xDLVO theories are often used to analyze and predict the scaling/fouling behavior on a liquid-solid interface [3]. For commonly used hydrophobic membranes, this assumption is valid as membrane pores are always in a Wenzel wetting state [43]. However, for a superhydrophobic surface which possesses a Cassie-Baxter wetting state, a water-air-solid tri-phase interface exists, which changes the paradigm of scaling kinetics. Many methods have been established to fabricate superhydrophobic membranes, however, substantial discrepancies in scaling resistance have been shown by these claimed “superhydrophobic” membranes [21, 43, 44]. It is suspected that different surface modification methods, either via chemical regent modification or CF4 physical modification, might contribute to the contrasting observations in MD. It is thus essential to conduct a side-by-side study of the potential difference of chemical and physical surface modification on MD scaling performance.

To achieve this, a tailor-made surface pillared PVDF microporous membrane (MP-PVDF) was selected as the model substrate [34]. This surface pattern allows us to estimate the surface wetting state via established methods [43]. 1H, 1H, 2H, 2H-perfluorodecyltriethoxysilane ((17-FAS) fluorination was implemented for chemical modification of the membrane surface, and CF4 plasma treatment for physical modification. Thermodynamic nucleation energy barrier and wetting state were analyzed to assess the potential scaling and behaviors. The slip lengths were measured to validate the wetting state of the membranes and the scaling behaviors of the membranes were compared using a supersaturated $CaSO_4$ solution. This research provides the first systematic investigation on the differences in MD performance between chemical and physical surface fluorination methods. The results indicate critically different effects on hydrodynamic wetting states that apparently similar surface modification methods can generate, and consequently significantly different anti-scaling performance.

2. Experimental methods

2.1 **Fabrication of MP-PVDF membrane**

The MP-PVDF membrane was fabricated following our previously established micro-molding phase separation (μPS) method [34], as illustrated in Fig.1. This includes (1) preparing a PDMS mold with a cylindrical hole array (Supplementary information S1), and (2) casting a PVDF solution against the PDMS mold followed by non-solvent induced phase separation (NIPS). PVDF solutions were prepared by mixing PVDF (Solvay, Solef ® PVDF 1015; 1.75~1.80 g/cm^3), diethylene glycol (DEG, purchased from Sinopharm, AR grade) and N, N-dimethylacetamide (DMAc, purchased from Sinopharm, AR grade) at a ratio of 15/27.4/57.6 in wt. % at 90 ºC for 8 h. Prior to casting, the polymer solutions were kept at 90 ºC for 12 h to remove air bubbles. With an appropriate amount of the solution

on the PDMS mold, a PVDF wet film of 500 μm thick was obtained and then exposed in water vapor (75 ºC±1) for 10 s. Exposure of the initial polymer solution was to allow adsorption of water vapour by the solvent in the solution. Subsequently, the nascent film on the PDMS mould was immersed into a water coagulation bath (75 ºC±1) to allow membrane precipitation [34]. Because of the pre-adsorption of water vapour, a non-solvent for PVDF, the polymer solution tend to demix rapidly, resulting in open pores to allow low mass transfer resistance. The as-prepared MP-PVDF membranes were rinsed with ethanol and water at least three times to remove residue solvents and additives, then dried at room temperature for 24 h.

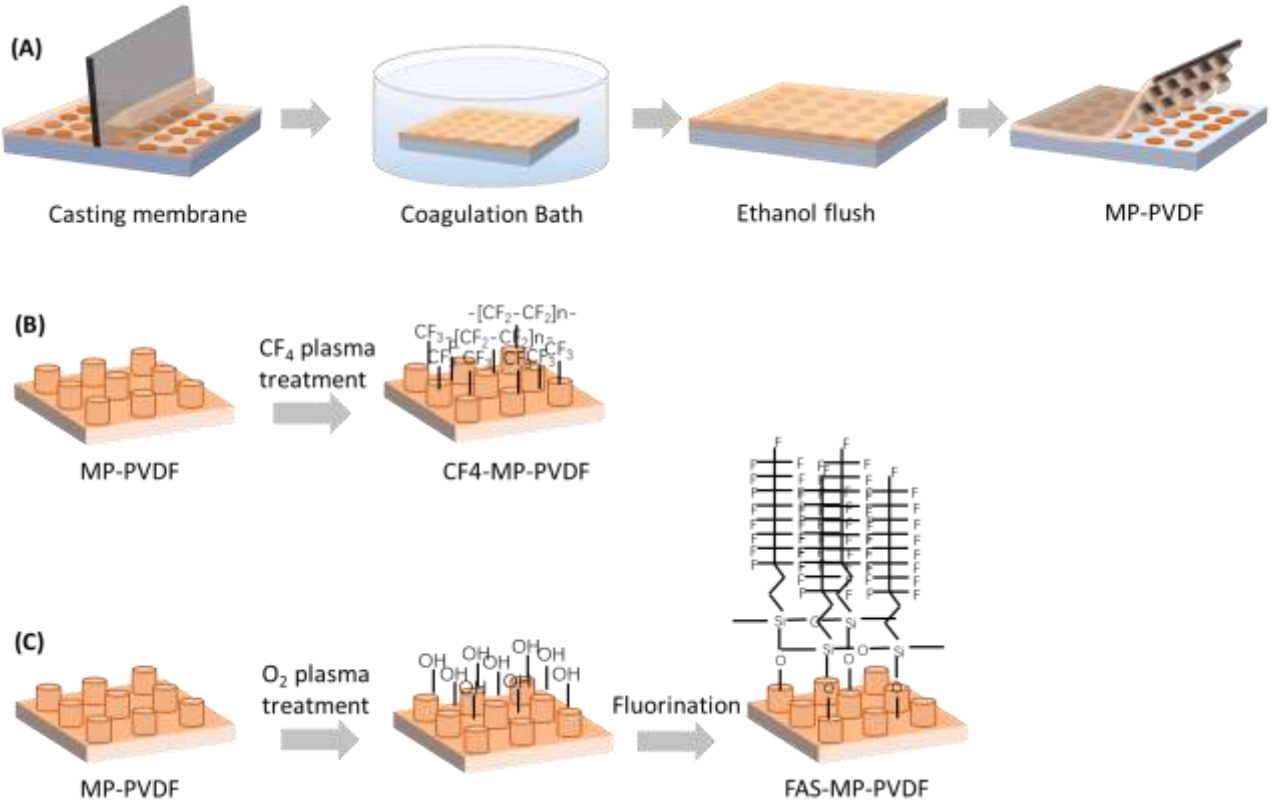

Fig. 1 (A) Schematic for preparation of MP-PVDF membrane via the non-solvent induced phase separation method. (B) Schematic for preparation of CF4-MP-PVDF membrane via CF4 plasma treatment. (C) Schematic for preparation of FAS-MP-PVDF membrane via chemical fluorination.

2.2 Surface modification

Two surface modification methods were employed to increase the hydrophobicity of MP-PVDF membranes (Fig. 1): (1) CF_4 plasma treatment and (2) liquid-phase silanization. The CF4 plasma treatment followed the optimized conditions in our previous study using an IoN40 plasma system (PVA Tepla Co. Ltd) [35]. Briefly, a clean MP-PVDF membrane was first treated with argon plasma at 45 W for 15 s, followed by CF_4 gas treatment at 200 W for 15 min. The modified membrane is denoted as CF_4-MP-PVDF. To chemically modify the surface, an MP-PVDF membrane was first treated with oxygen plasma at 50 W for 1 min to functionalize the membrane surface with hydroxyl groups before being immediately soaked in 1 % v/v 17-FAS (Sigma-Aldrich) in hexane at 65 ºC for 24 h. Afterwards, the modified MP-PVDF membranes were thoroughly rinsed with hexane and dried at 100 ºC for 1 h. The resultant membrane is denoted as FAS-MP-PVDF.

2.3 Membrane characterization

The mean pore size of membranes was analyzed using a capillary flow porometry (Porolux 1000) following a standard protocol [45]. The surface porosity was determined based on high resolution scanning electron microscopy (SEM) images using Image J software [43]. Surface morphology of the pristine and modified MP-PVDF membranes were examined using a HITACH TM-1000 SEM for low magnification or an FEI Nova Nano SEM 450 for high magnification. Before imaging, membrane samples were sputter-coated with a thin layer of gold to increase electrical conductivity. The elemental compositions of the pristine and modified membranes were analyzed by X-ray photoelectron

spectroscopy (Thermo, ESCALAB 250Xi) with a monochromatic Al Kα line (1486.6 eV).

Surface roughness of membranes was measured using a NanoWizard II Atomic Force Microscope (JPK Instruments). Prior to tests, a membrane sample was adhered to a glass slide and stored in an oven for 40 minutes at 70 ºC to remove any residual moisture in the membrane. Images were taken in intermittent contact mode with a silicon nitride cantilever (hq:nsc15, Mikromasch) with a nominal spring constant of 40 N/m and tip radius of 8 nm. Scan sizes of 50 x 50 μm and 5 x 5 μm were used to gain a view of the pillar array and detailed top surface of the pillars respectively.

Static water contact angle (CA) was measured using a contact angle goniometer (Maist Drop Meter A-100P) via the sessile drop method by placing a 5 μL water droplet on the membrane surface and taking images with a digital camera. All the measurements were performed at randomly selected areas on freshly prepared membranes. Contact angles of membranes for glycerol and diiodomethane were also measured to determine membrane surface energy (Supplementary Information S2). Contact angle hysteresis was evaluated by measuring the water sliding angle (SA), defined as the critical tilting angle at which the water droplet starts to roll off. Advancing angle was measured in two steps: first, a 5 μl water droplet was dropped on the membrane surface without pulling out the needle, then the second droplet was added to the first droplet while the syringe needle was immersed. The contact angle of the larger droplet (droplet is made up of two 5 μl droplets) is the advancing angle.

The slip length of the membranes were determined by torque measurement using a rheometer (AR-2000ex) [46]. A thermostatic controlled Peltier plate (base plate) was maintained at a constant temperature of 25±0.2 ºC. Three different membrane samples were carefully fixed to the base plate via tape, a stainless-steel cone plate with diameter of 50 mm and cone angle of 1 º was used to measure liquid viscosity on the three membranes, whose shear rate range was set at 10-100 (s^{-1}). The equipment

was pre-calibrated using deionized water. Deionized water and 20 wt.% glycerin solutions were chosen as the test liquids. Results of measurements and calculation procedure for slip length are reported in **Supplementary Information S3**.

2.4 Direct Contact Membrane Distillation (DCMD) performance

The membrane scaling behaviors were studied using a bench-scale DCMD unit, equipped with a custom-made acrylic double channeled DCMD cell (Length = 50 mm, Width = 20 mm, and Depth = 3 mm). Peristaltic pumps were used for both feed and distillate at a flow rate of 600 ml/min. Although $CaCO_3$ and $CaSO_4$ (Sigma-Aldrich) are often used to study scaling phenomena, the non-alkaline scalant $CaSO_4$ is selected in the study since its solubility is pH-independent. Supersaturated $CaSO_4$ solution (3000 mg/l, SI = 0.12) was prepared by mixing 22 mM Na_2SO_4 and 22 mM $CaCl_2$ following reference [17], the temperatures of the feed and distillate were maintained at 70 °C and 20 °C, respectively. Water vapor flux (J, $kg/m^2 \cdot h$) was determined by measuring the increased weight in distillate side over time. The electrical conductivity of the distillate was monitored using a calibrated conductivity meter. After DCMD experiments, the membranes were rinsed carefully using deionized water to remove residual feed liquid, then dried in ambient before further analysis.

3. Results and discussion

3.1 Membrane characterization

Both SEM and AFM images show all the membranes were highly porous (Fig 2). While the overview of surface morphology appeared similar for all the membranes (Fig. 2A), high resolution AFM imaging revealed subtle structural differences on the top surface of the micropillars between the

three membranes (Fig. 2C&D). The MP-PVDF membrane appeared to have mainly large pores whereases networks of small pores and small polymer nodules were observed in the FAS-MP-PVDF and CF4-MP-PVDF membranes (Fig. 2D). For FAS-MP-PVDF, smaller pores are likely due to the coated layer of fluoroalkyl silane on the existing pores, which was indicated by the apparent reduction in surface roughness (Supplementary Information S4) compared to the other two membranes. For CF4-MP-PVDF, the newly formed smaller pores are likely caused by CF4 etching [35]. Therefore, although no significant differences were found in the average pore size determined by the bulk measurement (i.e. capillary flow porometry) (Table 1), the network of porous structures at the microscale level was clearly modified differently by both treatments.

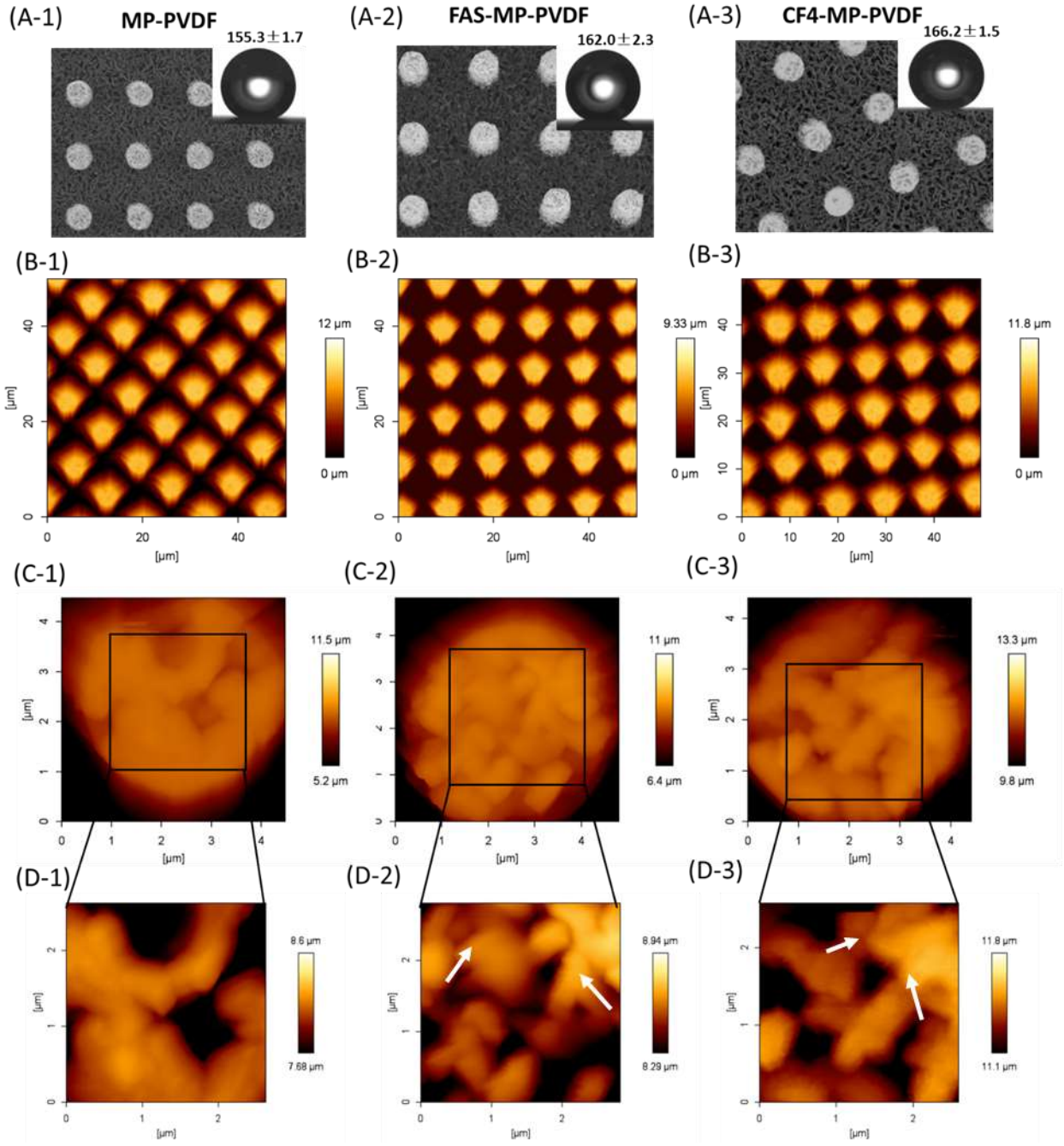

182

183 Fig. 2 (A) Top view and static contact angle of the pristine and modified membranes. AFM images of

184 (B) pillar array, (C) single pillar, and (D) zoom area on top of a single pillar of the pristine and

185 modified membranes. The dark areas in AFM images represent depressions and pores. White arrows

186 indicate small polymer nodules.

187

188 Table 1. Characteristics of the MP-PVDF, FAS-MP-PVDF and CF4-MP-PVDF membranes.

Membrane	MP-PVDF	FAS-MP-PVDF	CF_4-MP-PVDF
Mean pore size/μm*	0.129±0.003	0.122±0.008	0.124±0.016
Water contact angle/°	155.3±1.7	162.0±2.3	166.2±1.5
Sliding angle/°	27.5±4.4	14.3±1.2	3.0±0.8
Advancing angle/°	157.3±1.0	164.1±1.6	169.6±1.5
Surface energy γ/mJ·m^{-2}	33.72±3.10	0.16±0.15	0.46±0.25
F1s	51.94	60.17	66.17
C1s	46.79	30.99	31.89
O1s	1.26	5.06	1.95
Si2p	0	3.78	0

189 *Determined by capillary flow porometry.

190

191 XPS spectra for the MP-PVDF, FAS-MP-PVDF and CF4-MP-PVDF membranes are shown in Fig.
192 3. Fluorine (F) and carbon (C) are the main elements of three membranes because PVDF contains only
193 C and F (Fig. 3A). However, the intensity of elements changed after surface modification (Table 1).
194 The proportion of fluorine (F) increased from 51.94% (MP-VPDF) to 60.17% (FAS-MP-VPDF) and
195 66.17% (CF4-MP-VPDF); this follows the increase in F/C ratio. For the FAS-MP-PVDF membrane,
196 Silicon (Si) and oxygen (O) are attributed to 17-FAS, as well as partially to the PDMS stamp and air.
197 Deconvolution of the core level C1s peak for MP-PVDF revealed that the carbon signals at 284.8
198 eV, 289.3 eV are mainly associated with C-C and $(-CH_2-CHF-)_n$. For the FAS-MP-PVDF membrane,

the chemical state of the carbon has changed, the C1s signal at 284.8 eV is adventitious carbon C-C, which was not affected by fluorination. However, the C1s signals at 285.97 eV, 291.3 eV and 293.64 eV correspond to C, CF_2 and CF_3, which were derived from the fluorinating reagents, indicating that the fluorinated coating was successful. The CF4-MP-PVDF membrane showed 7 C1s signals, the dominant signal at 289.92 eV refers to CF_2-CF_2, other signals at 288 eV, 291.82 eV, 285.97 eV, 294.05 eV correspond to $(-CHFCHF-)_n$, $(-CF_2-CF_2-)_n$, $(-CH_2CF_2-)_n$, CF_3 respectively. These indicate that the CF4 plasma treatment took place by deposition and replacement of segments of fluoride. Both the chemical and physical modification methods indeed changed the chemical states of carbon and introduced more fluorine. How these changes impact on membrane performance is yet to be elaborated.

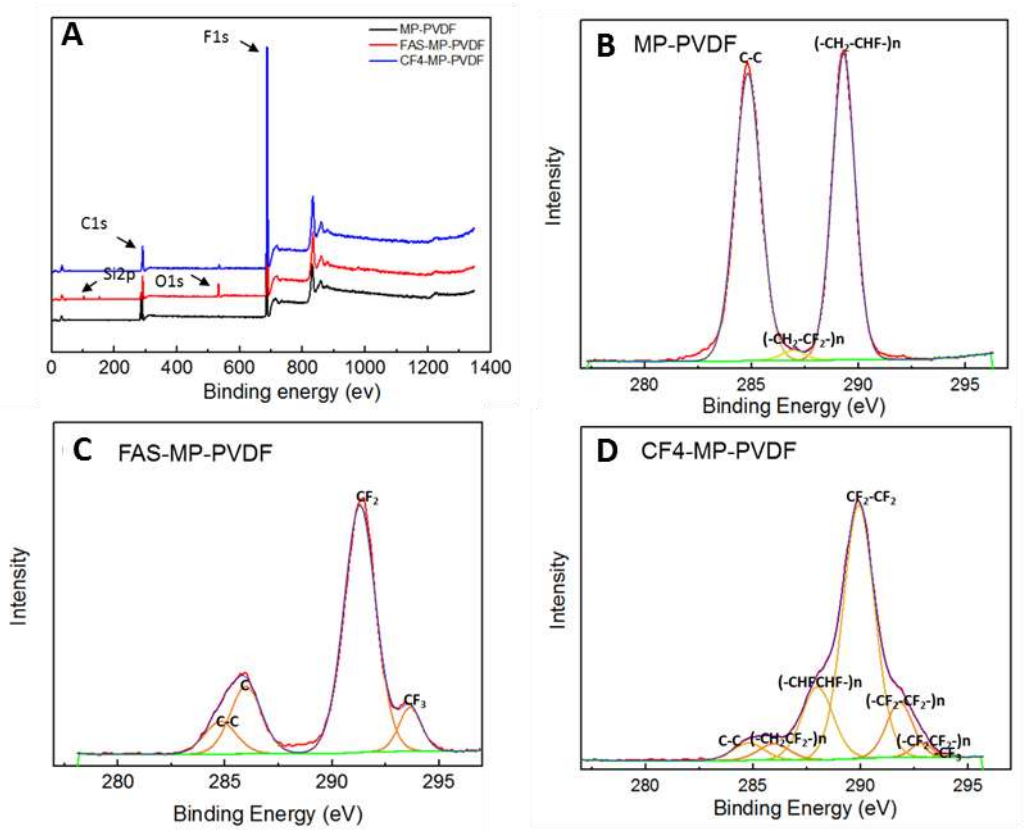

Fig. 3 (A) X-ray photoelectron spectroscopy (XPS) survey scan spectra of the MP-PVDF, FAS-MP-PVDF and CF4-MP-PVDF. (B), (C), (D) are deconvolution of the core level C1s spectra of MP-

PVDF, FAS-MP-PVDF, CF4-MP-PVDF membranes, respectively.

The static water contact angles of three membranes are shown in Fig. 4A. As expected, the increase of fluoride composition in the modified membranes increased the contact angles and thus the hydrophobicity. In comparison to MP-PVDF (i.e. water contact angle of 155 ^{o}), the static contact angles of both modified membranes were above 160 ^{o}, with that of CF4-MP-PVDF slightly higher. However, the sliding angle of FAS-MP-PVDF (14.3 ^{o}) was significantly higher than that of CF4-MP-PVDF (3 ^{o}). The contact angles of glycerol and diiodomethane on the membrane were also measured for surface energy calculation (Fig. 4A). The modified membranes exhibited higher contact angles for diiodomethane and glycerol than that of MP-PVDF, and thus significantly reduced surface energies (i.e. 0.16 $mJ \cdot m^{-2}$ for FAS-MP-PVDF, 0.46 $mJ \cdot m^{-2}$ for CF4-MP-PVDF, in comparison to 33.72 $mJ \cdot m^{-2}$ for MP-PVDF, table 1). This further proves the successful incorporation of fluoroalkyl chains of 17-FAS or fluoride chain segments to the modified membrane. FAS-MP-PVDF shows similar higher contact angles compared to CF4-MP-PVDF (Table 1), but the latter had a lower sliding angle than FAS-MP-PVDF (Table 1, Fig.4B). Sliding angle has been utilized as a qualitative measure for the slippage of a hydrophobic surface [18]. Therefore, the large variation in sliding angles for different membranes is a clear indication that CF4-MP-PVDF appears to be slippery compared to MP-PVDF as well as FAS-MP-PVDF.

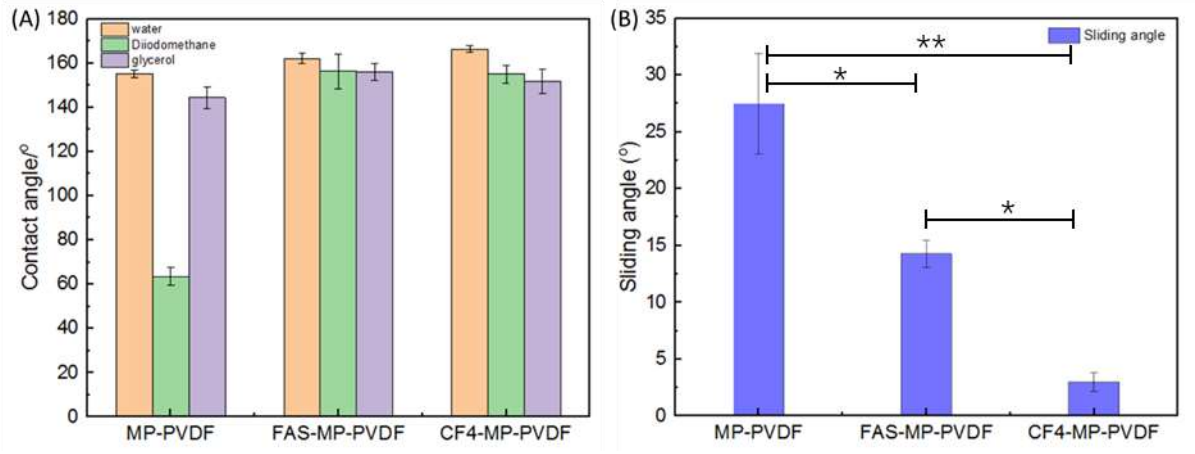

229

230 Fig. 4 (A) Contact angles of three membranes for water, diiodomethane and glycerol,

231 respectively. (B) Sliding angles of three membranes for water.

232

233 **3.2 Scaling behavior in DCMD process**

234 Scaling performance of three membranes were compared as shown in Fig.5. The initial flux for

235 MP-PVDF and CF4-MP-PVDF was very similar at 31.2 kg/m^2·h and 32.1 kg/m^2·h, respectively but

236 the flux of FAS-MP-PVDF was 21.6 kg/m^2·h. Chemical surface fluorination by FAS leading to reduced

237 initial flux has been demonstrated previously [47], showing that the fluorinated coating can increase

238 wetting resistance, and impede deeper penetration of the liquid−air interfaces into the membrane,

239 resulting in a decreased interfacial area and therefore a decreased flux in comparison to MP-PVDF [47].

240 As shown in Fig.5A, the flux of MP-PVDF (green square) declined gradually after a short induction

241 time. The flux of FAS-MP-PVDF initially declined in a similar magnitude to MP-PVDF, but less than

242 MP-PVDF after the concentration factor reached 1.3. The most stable performance was found for CF4-

243 MP-PVDF as the flux only decreased slightly beyond a concentration factor of 1.4. It should be noted

244 that the initial feed solution was a supersaturated $CaSO_4$ solution. The concentration factor less than

245 1.1 was an induction period with a stable flux. Above this value, nuclei may form, most probably on

246 the membrane surface via heterogeneous nucleation [48], consequently the flux declined as shown in Fig.

5A for MP-PVDF. Thermodynamic analysis of nucleation energy showed similar, high Gibbs free energy for the three membranes (Fig. 6A), however, their scaling behaviors were different. The pinned wetting state (Fig.6B) and negative slip length (Fig.7) indicated that the surface of MP-PVDF was in a Wenzel state which meant that water actually imbedded within the porous pillars. The presence of nuclei both in the bulk solution and on the membrane surface was highly likely after the induction period as shown by the quick decline in the MD flux above a concentration factor of 1.1 (Fig. 5A).

FAS-MP-PVDF showed a similar scaling resistance to MP-PVDF, which was unexpected. Evaluation of the wetting state suggested that FAS-MP-PVDF was in an unstable transition state (Fig.6B), which tended to shift to a pinned wetting state during the MD process. In contrast, CF4-MP-PVDF was in a suspended wetting state, which is believed to account for its robust MD performance. As shown in Fig.5A, the flux of CF4-MP-PVDF only dropped by 20 % at a concentration factor of 1.45 compared to > 50% reduction for MP-PVDF and FAS-MP-PVDF membranes. SEM images of the membrane surface after the experiment (Fig.5B) are in line with the observed MD flux pattern: The CF4-MP-PVDF membrane showed rather a clean surface with sporadic deposition of crystals, but MP-PVDF and FAS-MP-PVDF surfaces are covered with many crystals. We have previously shown that large crystal aggregates can penetrate the membrane, contributing to membrane wetting [17]. Although both FAS-MP-PVDF and CF4-MP-PVDF have similar static contact angles, surface energy and nucleation energy barrier, the scaling behavior was significantly different. The consequence of the calcium sulfate scaling includes the reduced hydrophobicity as we observed that a thin layer of water adhered closely to the membrane surface after taking out the membrane from the test module. For samples fully covered with calcium sulfate, mechanical strength was reduced as well. Previous studies show that substantial deposition of calcium sulfate crystals can destroy porous membranes and cause

wetting [49, 50].

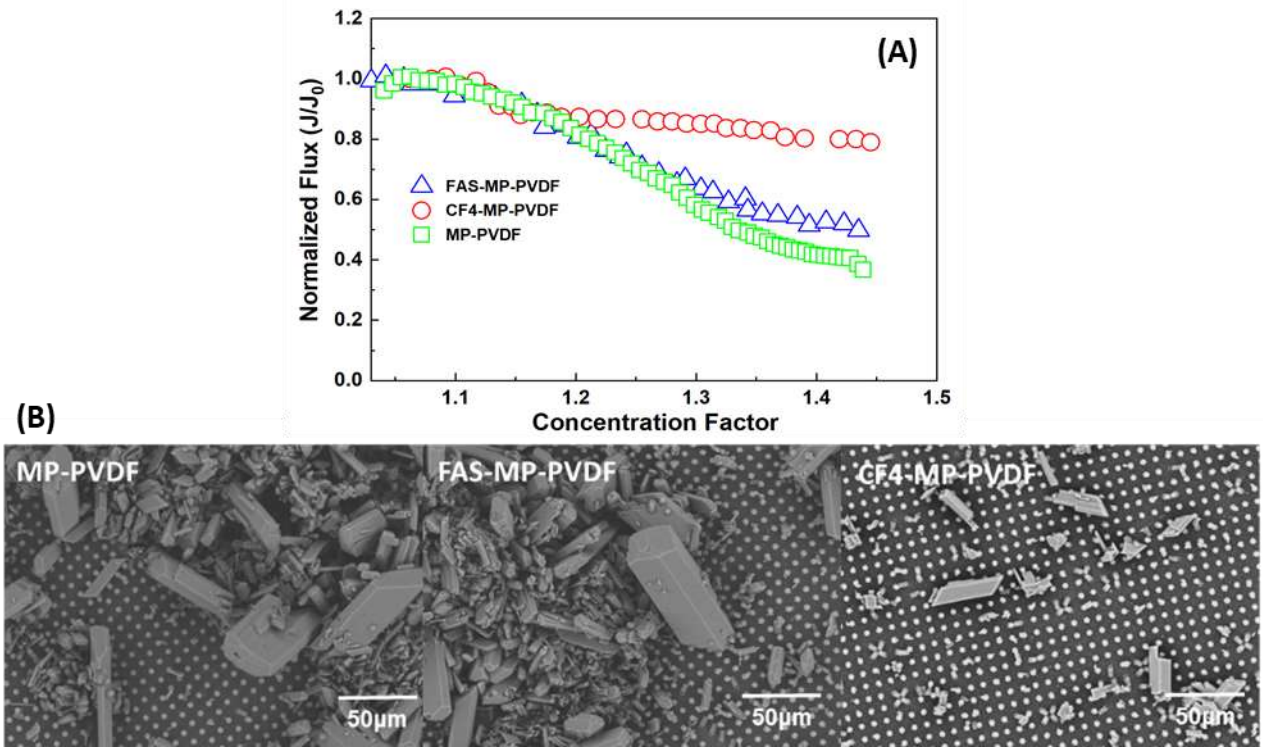

Fig. 5 (A) Normalized flux as a function of concentration factor for MP-PVDF, FAS-MP-PVDF, CF4-MP-PVDF membranes. The feed solution contained 22 mM Na_2SO_4 and 22 mM $CaCl_2$, and the initial volume was 1.2 L. The temperature at the feed side was 70 ºC and permeate was 20 ºC. the circulation rates of the peristaltic pump were 600 ml/min. the initial flux of MP-PVDF, FAS-MP-PVDF and CF4-MP-PVDF was 31.2 kg/m^2·h, 21.6 kg/m^2·h, 32.1 kg/m^2·h, respectively. (B) SEM images of the membrane surfaces after $CaSO_4$ scaling experiments.

3.3 Scaling potential: thermodynamic analysis and wetting state

In a membrane process, heterogeneous nucleation requires a smaller Gibbs free energy compared to homogeneous nucleation [7, 48]. Classical nucleation theory (CNT) explains the influence of surface

properties on heterogeneous nucleation of calcium sulfate. According to the CNT, formation of nuclei should overcome certain energy barriers, and enough contact time for nuclei at the interface between liquid and membrane surface is necessary for crystal growth and deposition. The energy barrier for heterogeneous surface nucleation corresponds to the homogeneous nucleation ($\Delta G^*_{homogeneous}$) by incorporating surface porosity and hydrophobicity [51, 52].

$$\Delta G^*_{heterogeneous} = \Delta G^*_{homogeneous}\left[\frac{1}{4}(2+\cos\theta)(1-\cos\theta)^2\right]\left[1-\varepsilon\frac{(1+\cos\theta)^2}{(1-\cos\theta)^2}\right]^3 \quad (1)$$

where θ is the membrane-liquid contact angle and ε is the membrane surface porosity. $\Delta G^*_{heterogeneous}$indicating that a membrane with higher hydrophobicity and lower surface porosity will exhibit lower scaling potential.

Fig. 6A presents the heterogeneous nucleation energy for MP-PDVF (26.97 mJ/mol), FAS-MP-PVDF (27.21 mJ/mol), CF4-MP-PVDF (27.27 mJ/mol). Obviously, the three membranes show very similar heterogeneous nucleation energy. Thus, one may expect that from thermodynamic analysis, all three should show a very similar scaling potential.

However, the CNT model neglects the location of the water-air-solid tri-phase interface, where scaling occurs. There are three types of wetting states [53]: 1) Droplets are embedded in the membrane, named Wenzel state or pinned-state. 2) droplets are supported by microstructures and hang on the membrane surface, which is called suspended wetting state (Cassie-Baxter state). 3) A metastable state in between the two mentioned above called transition state. For a micropillared surface, a wetting state factor may be used to evaluate the wetting states as defined below [53]:

$$\zeta = \frac{(\sqrt{2}S_f-1)}{2a_r}\tan(\theta_a-\varphi) \quad (2)$$

where $S_f = \frac{p}{D}$, indicates the spacing factor (Supplementary information S5), and $a_r = \frac{H}{D}$, is the

aspect ratio given by the height and diameter of a pillar on the membrane. θ_a is the advancing angle and φ is the interior angle as a geometrical factor ($\varphi = 90°$ for cylindrical pillars). $\zeta < 0.5$ corresponds to a Cassie-Baxter state, $\zeta > 0.75$ for Wenzel state, whereas a transition state is at $0.75 > \zeta > 0.5$.

Although all three membranes showed high static water contact angles (>150°), they were in different wetting states. Fig 6B depicts that MP-PVDF was in a pinned state, CF_4-MP-PVDF was in a suspended wetting (Cassie-Baxter) state, and FAS-MP-PVDF was in a transition state. The transition state was unstable, thus converting to a pinned state when the external pressure changed. In a suspended state, the air-liquid interface is supported on the top of pillars consisting of a small liquid-membrane contact area. Consequently, the probablility for scalants to contact the solid area (membrane surface) is limited. In contrast, a pinned-state means the air-liquid interface sinks into the pillars and the contact area between liquid and membrane is large, allowing more sites for nuclei growth or deposition, thus leading to severe scaling.

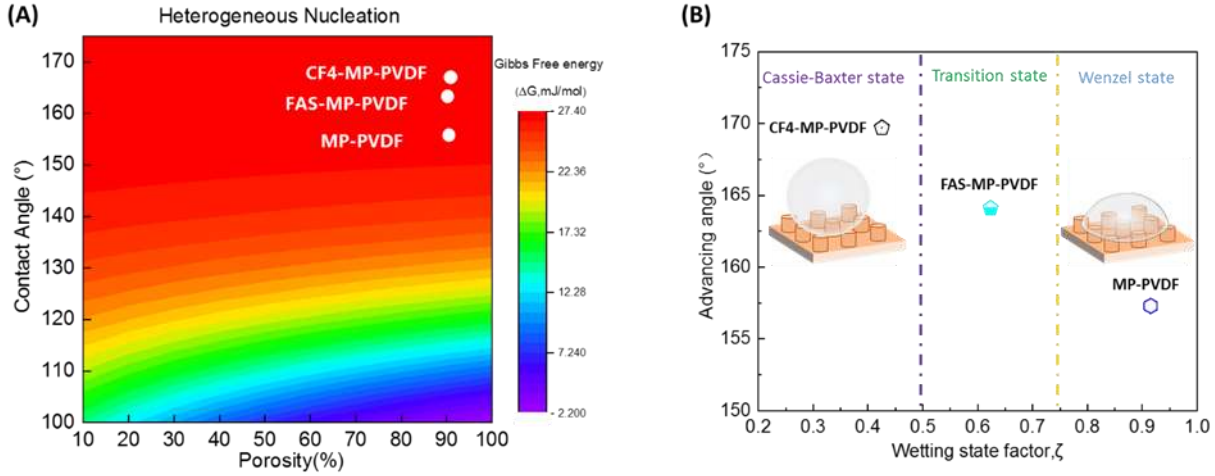

Fig.6 (A) Map of Gibbs free energy for heterogeneous nucleation of CaSO4. white dots represent the energy barriers of the three membranes. (B) Map of the wetting state factor for MP-PVDF, FAS-MP-PVDF, CF4-MP-PVDF membranes.

3.4 Slip length

Wetting state analysis considers a static state where no external force is applied. However, in a real membrane process, flow naturally exerts a force onto the water-air-solid interface. Thus, it is of practical importance to analyze the hydrodynamic wetting state to mimic a real scenario. For this purpose, we have recently introduced a slip length measurement [43]. When a fluid flows tangentially to a membrane surface, it is generally assumed that the liquid velocity at the water-membrane interface is zero, called the non-slip assumption [54, 55]. However, it has been proven that for a superhydrophobic surface, considerable air pockets exists at the interface, which may invalidate the non-slip assumption and induce slip [56]. This suggests that the liquid velocity at the interface is not zero (Supplementary Information S3 for detailed description). By measuring the slip length at flow with low external pressure applied (Supplementary Information S3), the wetting state of a membrane surface can be determined.

With deionized water and 20 wt.% glycerol solutions as the probe liquids, the slip length of the three membranes at varying shear rates were obtained (Fig. 7). The MP-PVDF membrane had a negative slip length, which decreased as the shear rate increased; this further suggests liquid sinking into the micropillars during the MD process. Both CF4-MP-PVDF and FAS-MP-PVDF had a positive slip length, suggesting that both membranes have slippery behavior. However, CF4-MP-PVDF in a suspended wetting state had a larger slip length than FAS-MP-PVDF, thus showing a greater slippery tendency. It's worth noting that with the increase of shear rate, the slip length for FAS-MP-PVDF was initially constant but then slightly decreased at higher shear rates, representing an instable transition state which may transform into a pinned state.

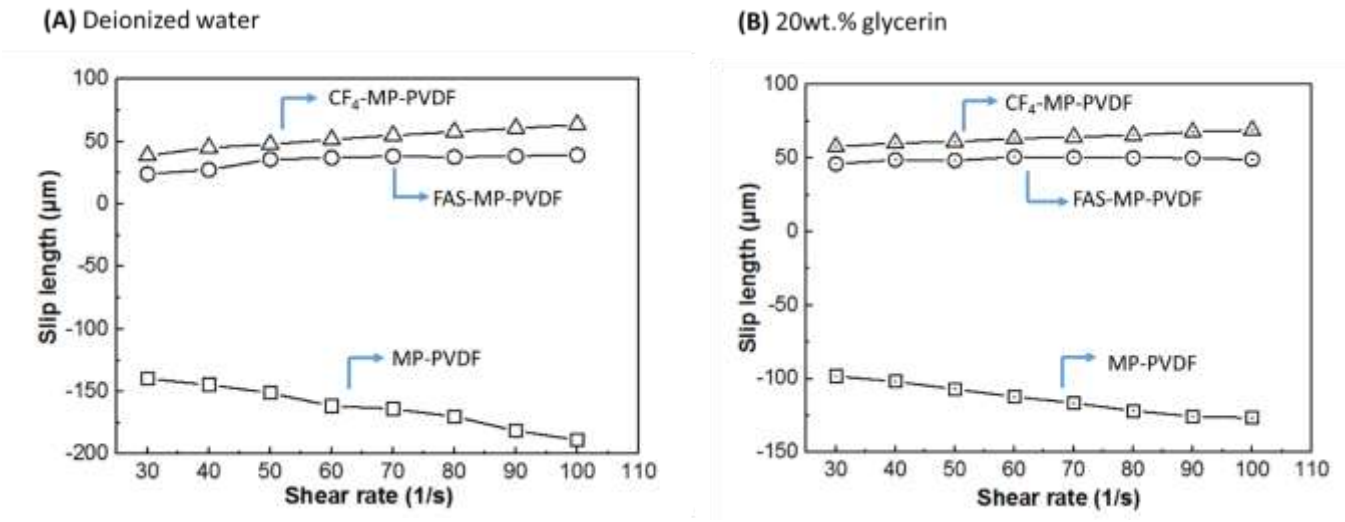

Fig.7 Slip length of MP-PVDF, FAS-MP-PVDF, CF4-MP-PVDF membranes corresponding to shear rate varying from 30 s^{-1} to 100 s^{-1}. (A) Deionized water is used as test liquid. (B) 20 wt.% glycerin is used as test liquid.

Wetting state analysis and slip length calculations overcome the shortcomings of classical thermodynamics, with contact angle only reflecting a membrane's characteristics in a static situation. However, during the MD operation, parameters such as sliding angle correlating to dynamic properties of membrane-liquid interface are also very important. Fig. 8 shows a cartoon description for the origin of the difference in scaling resistance for both CF4-MP-PVDF and FAS-MP-PVDF membranes. Although both fluorination methods attribute surface chemical modification to a MP-PVDF membrane, CF4 plasma contributes to suspended wetting (Fig. 8 top), thus a slippery surface which is scaling resistant. Flurosilane modification based on only chemical treatment results in a transition wetting state, which easily transforms to a pinned wetting state and is thus not scaling resistant.

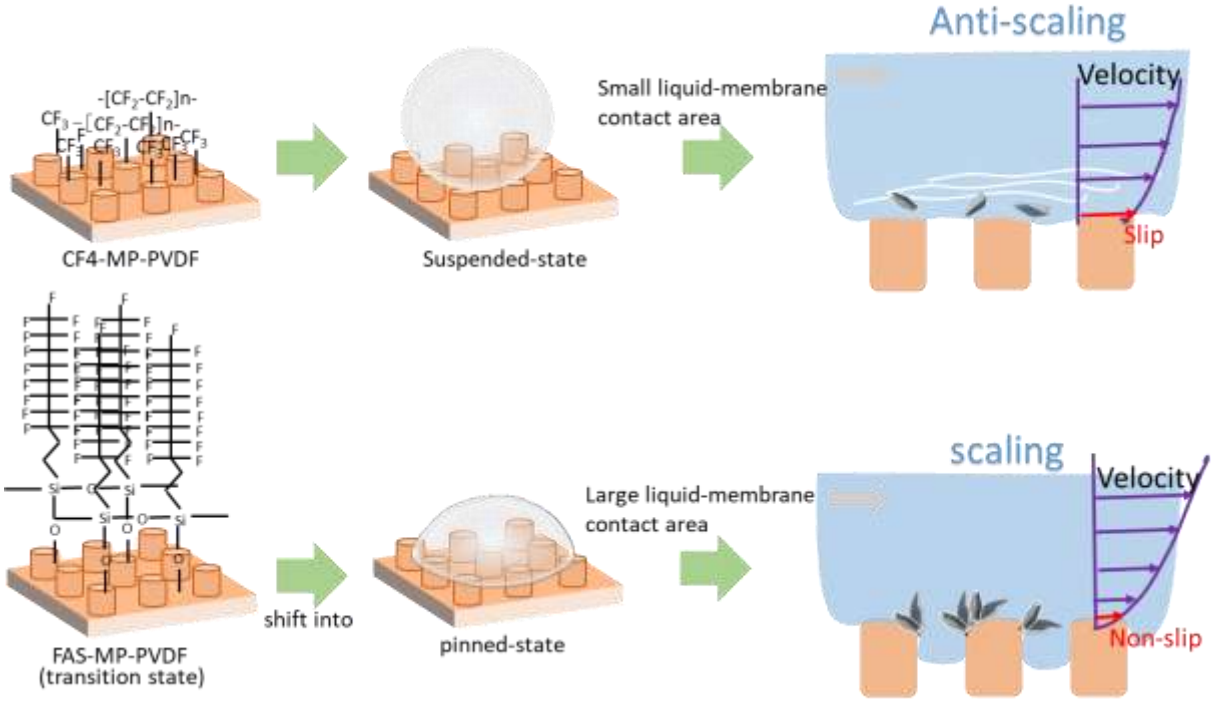

Fig. 8 Schematic diagram for the correlation among wetting state, slip length and scaling resistance.

Obvious contrast in the wetting states for CF4-MP-MVDF and FAS-MP-PVDF membranes probably stems from the difference in the top surface microstructure. The MP-PVDF top surface (pillars) showed large pores (Fig. 2D); FAS-MP-PVDF showed smaller pores because of the fluoroalkyl silane coating, which also resulted in an apparent reduction in surface roughness (Supplementary Information S4). For CF4-MP-PVDF, CF4 etching contributed to smaller pores [35] and a slightly roughened top surface (Fig. 2 C/D-2 and C/D-3). The small variation is most probably due to the deposition and replacement of segments of fluoride during CF4 plasma treatment, which is drastically different from the FAS treatment via chemical modification. Consequent analysis of the water contact angle, the sliding angle, as well as the slip length and scaling resistance, suggest a coherent design strategy of scaling resistant hydrophobic membranes. The porosity, roughness and

surface chemistry are key factors to create a surface with slippage and suspended wetting, thus achieving improved scaling resistance. Other process parameters, such as pulse flow, nanobubbles, antiscalant chemicals etc., may be combined with the membrane development to realize extended scaling resistance in a membrane distillation process for concentrating high salinity streams.

4. Conclusions

The difference in scaling resistance of a porous micropillared PVDF membrane modified by chemical fluorination or CF4 plasma treatment was systematically investigated. Both methods successfully generated fluorinated groups on the membrane surface. Macroscopic characterization of the membrane surface revealed that both modified membranes showed similarly enhanced static contact angles and reduced surface energy. However, CF4-MP-PVDF outperformed FAS-MP-PVDF membranes in scaling resistance with a flux decline below 20 %, whereas the flux of FAS-MP-PVDF dropped by more than 50%. Classical thermodynamic analysis suggested that the three membranes should have a similar energy barrier, contrary to the observation. However, hydrodynamic analysis indicated that CF4-MP-PVDF was in a suspended wetting state and had a slippery surface, resulting in its excellent scaling resistance. The transition wetting state of FAS-MP-PVDF tends to transform to a pinned wetting state, which is similar to MP-PVDF and is thus not scaling resistant. Although the macroscopic properties of the membranes can’t explain the surprising phenomena of differing scaling resistance, the microscopic networks of submicron-micropores generated by the two methods might shed more light. These clear differences in the network structure and resultant surface roughness mean these performance differences could be amplified considering the substantial surface area offered by the 3D micro-pillars arrays. However, this lays beyond the scope of this study. Nevertheless, this

finding demonstrates that small difference in surface fluorination, fluorisaline and CF4 plasma treatments, can cause different wetting state of superhydrophobic membranes. Although the results reveal that a suspended wetting state play an important role in scaling resistance, the application of such a concept to a large scale membrane modules is still challenging. For a large module, it has been reported that the saturation index at the vicinity of the membrane surface is significantly greater than that in the bulk because of both concentration and temperature polarization [57]. Critical analysis via simulation would give more insight into this issue. Other process parameters, such as pulse flow, nanobubbles, antiscalant chemicals etc., may be combined with the membrane development to realize extended scaling resistance in a membrane distillation process for concentrating high salinity streams.

Conflicts of interest

There are no conflicts to declare.

Acknowledgements

The research was partially supported by National Natural Science Foundation of China (No. 21978315, 52011530031, 21764011), Royal Society Newton Advanced Fellowship (No. NA170113) EPSRC SoftMech (EP/N014642/1), and CAS International Collaboration (No. GJHZ2080). We also thank the frame work research consortium BRICS for financial support (RFBR No. 18-58- 80031, NSFC No. 51861145313, DST IPN/7864, NRT No.116020, CNPq/BRICS-STI-2-442229/2017–8).

References

1. A. Alkhudhiri, N. Darwish and N. Hilal, *Desalination*, 2012, **287**, 2-18.
2. M. S. El-Bourawi, Z. Ding, R. Ma and M. Khayet, *J. Membr. Sci.*, 2006, **285**, 4-29.
3. L. Liu, Z. Xiao, Y. Liu, X. Li, H. Yin, A. Volkov and T. He, *Desalination*, 2021, **499**.
4. T. Horseman, Y. Yin, K. S. S. Christie, Z. Wang, T. Tong and S. Lin, *ACS ES&T Engineering*, 2021, **1**, 117-140.

5. T. Z. Tong and M. Elimelech, *Environ. Sci. Technol.*, 2016, **50**, 6846-6855.
6. T. Z. Tong, A. F. Wallace, S. Zhao and Z. Wang, *J. Membr. Sci.*, 2019, **579**, 52-69.
7. Y. Chen, K. J. Lu and T.-S. Chung, *J. Membr. Sci.*, 2020, **595**, 117572.
8. W.-Y. Shih, A. Rahardianto, R.-W. Lee and Y. Cohen, *J. Membr. Sci.*, 2005, **252**, 253-263.
9. Y. Peng, J. Ge, Z. Li and S. Wang, *Separation and Purification Technology*, 2015, **154**, 22-26.
10. F. He, K. K. Sirkar and J. Gilron, *J. Membr. Sci.*, 2009, **345**, 53-58.
11. M. Gryta, *Desalination*, 2012, **285**, 170-176.
12. J. Wang, D. Qu, M. Tie, H. Ren, X. Peng and Z. Luan, *Separation and Purification Technology*, 2008, **64**, 108-115.
13. W. Zhang and X. Zhang, *J. Membr. Sci.*, 2021, **632**, 119358.
14. E. H. Kelle Zeiher, B. Ho and K. D. Williams, *Desalination*, 2003, **157**, 209-216.
15. M. Badruzzaman, N. Voutchkov, L. Weinrich and J. G. Jacangelo, *Desalination*, 2019, **449**, 78-91.
16. S. H. Park, J. H. Kim, S. J. Moon, J. T. Jung, H. H. Wang, A. Ali, C. A. Quist-Jensen, F. Macedonio, E. Drioli and Y. M. Lee, *J. Membr. Sci.*, 2020, **598**, 117683.
17. L. Liu, H. He, Y. Wang, T. Tong, X. Li, Y. Zhang and T. He, *J. Membr. Sci.*, 2021, **624**, 119107.
18. Y. Liu, Z. Li, Z. Xiao, H. Yin, X. Li and T. He, *J. Membr. Sci*, 2020, **603**, 118035.
19. G. Z. Chen, X. Yang, R. Wang and A. G. Fane, *Desalination*, 2013, **308**, 47-55.
20. Y. Ye, S. Yu, L. a. Hou, B. Liu, Q. Xia, G. Liu and P. Li, *Water Research*, 2019, **149**, 588-595.
21. T. Horseman, C. Su, K. S. S. Christie and S. Lin, *Environmental Science & Technology Letters*, 2019, **6**, 423-429.
22. X. M. Li, D. Reinhoudt and M. Crego-Calama, *Chem Soc Rev*, 2007, **36**, 1350-1368.
23. W. H. Qing, Y. F. Wu, X. H. Li, X. N. Shi, S. L. Shao, Y. Mei, W. Zhang and C. Y. Y. Tang, *J. Membr. Sci.*, 2020, **608**, 7.
24. C. Su, T. Horseman, H. Cao, K. Christie, Y. Li and S. Lin, *Environ. Sci. Technol.*, 2019, **53**, 11801-11809.
25. M. Xie, W. Luo and S. R. Gray, *Water Research*, 2017, **124**, 238-243.
26. A. Razmjou, E. Arifin, G. Dong, J. Mansouri and V. Chen, *J. Membr. Sci.*, 2012, **415**, 850-863.
27. E. J. Lee, B. J. Deka, J. Guo, Y. C. Woo, H. K. Shon and A. K. An, *Environ. Sci. Technol.*, 2017, **51**, 10117-10126.
28. Y. Liao, G. T. Zheng, J. J. Huang, M. Tian and R. Wang, *J. Membr. Sci.*, 2020, **601**, 117962.
29. Z. Xiao, H. Guo, H. He, Y. Liu, X. Li, Y. Zhang, H. Yin, A. V. Volkov and T. He, *J. Membr. Sci.*, 2020, **599**, 117819.
30. Z. Zhu, L. Zhong, T. Horseman, Z. Liu, G. Zeng, Z. Li, S. Lin and W. Wang, *J. Membr. Sci.*, 2020, **620**, 118768.
31. C. Boo, J. Lee and M. Elimelech, *Environ Sci Technol*, 2016, **50**, 12275-12282.
32. C. Boo, J. Lee and M. Elimelech, *Environ Sci Technol*, 2016, **50**, 8112-8119.
33. S. Lin, S. Nejati, C. Boo, Y. Hu, C. O. Osuji and M. Elimelech, *Environ Sci Technol Letters*, 2014, **1**, 443-447.
34. Z. Xiao, R. Zheng, Y. Liu, H. He, X. Yuan, Y. Ji, D. Li, H. Yin, Y. Zhang, X. M. Li and T. He, *Water Research*, 2019, **155**, 152-161.
35. C. Yang, X.-M. Li, J. Gilron, D.-f. Kong, Y. Yin, Y. Oren, C. Linder and T. He, *J. Membr. Sci.*, 2014, **456**, 155-161.
36. H. Kyong Shon, *J. Membr. Sci.*, 2017, **529**, 234-242.
37. F. Zhao, Z. Ma, K. Xiao, C. Xiang, H. Wang, X. Huang and S. Liang, *Desalination*, 2018, **443**, 228-236.
38. L.-H. Chen, A. Huang, Y.-R. Chen, C.-H. Chen, C.-C. Hsu, F.-Y. Tsai and K.-L. Tung, *Desalination*, 2018, **428**, 255-263.
39. X. Li, W. Qing, Y. Wu, S. Shao, L. E. Peng, Y. Yang, P. Wang, F. Liu and C. Y. Tang, *Applied Materials & Interfaces*, 2019, **11**, 47963-47971.
40. R. D. Saikat Sinha Ray, Young-Nam Kwon, *Chemical Engineering Journal*, 2021, **405**, 126702.
41. C. Yang, M. M. Tian, Y. M. Xie, X. M. Li, B. L. Zhao, T. He and J. D. Liu, *J. Membr. Sci.*, 2015, **482**, 25-32.
42. S. Meng, Y. Ye, J. Mansouri and V. Chen, *J. Membr. Sci.*, 2015, **473**, 165-176.
43. Z. Xiao, Z. Li, H. Guo, Y. Liu, Y. Wang, H. Yin, X. Li, J. Song, L. D. Nghiem and T. He, *Desalination*, 2019, **466**, 36-43.
44. V. Karanikola, C. Boo, J. Rolf and M. Elimelech, *Environ Sci Technol*, 2018, **52**, 14362-14370.
45. X. Wei, B. Zhao, X.-M. Li, Z. Wang, B.-Q. He, T. He and B. Jiang, *J.Membr.Sci*, 2012, **407-408**, 164-175.

46. C. H. Choi and C. J. Kim, *Phys. Rev. Lett.*, 2006, **96**, 4.
47. C. Li, X. Li, X. Du, Y. Zhang, W. Wang, T. Tong, A. K. Kota and J. Lee, *Environ Sci Technol*, 2020, **54**, 10333-10341.
48. G. Di Profio, E. Curcio and E. Drioli, *Industrial & Engineering Chemistry Research*, 2010, **49**, 11878-11889.
49. Y. M. Yin, N. Jeong and T. Z. Tong, *J. Membr. Sci.*, 2020, **614**.
50. Y. M. Yin, W. Wang, A. K. Kota, S. Zhao and T. Z. Tong, *Environ Sci-Wat Res*, 2019, **5**, 2004-2014.
51. E. Curcio, X. S. Ji, G. Di Profio, A. Sulaiman, E. Fontananova and E. Drioli, *J. Membr. Sci.*, 2010, **346**, 263-269.
52. E. Curcio, E. Fontananova, G. Di Profio and E. Drioli, *J. Phys. Chem. B*, 2006, **110**, 12438-12445.
53. H. S. Grewal, I.-J. Cho, J.-E. Oh and E.-S. Yoon, *Nanoscale*, 2014, **6**, 15321-15332.
54. C. Navier, *Mémoires de l'Académie Royale des Sciences de l'Institut de France*, 1823, **6**, 389-440.
55. B. M. P. Lauga E, Stone H A., *Microfluidics: The no-slip boundary condition*, Springer, NewYork, 2005.
56. J. Li, M. Zhou, L. Cai, X. Ye and R. Yuan, *Chinese Science Bulletin*, 2009, **54**, 4560-4565.
57. S. Soukane, H. Elcik, A. Alpatova, J. Orfi, E. Ali, H. AlAnsary and N. Ghaffour, *Journal of Cleaner Production*, 2021, **287**, 125555.